Acta Biomaterialia 174 (2024) 163–176

Contents lists available at ScienceDirect

Acta Biomaterialia

journal homepage: www.elsevier.com/locate/actbio

Full length article

Scaffolded spheroids as building blocks for bottom-up cartilage tissue engineering show enhanced bioassembly dynamics

Oliver Kopinski-Grünwald[a,b,1], Olivier Guillaume[a,b,1,*], Tamara Ferner[a,b], Barbara Schädl[b,c,d], Aleksandr Ovsianikov[a,b,*]

[a] 3D Printing and Biofabrication Group, Institute of Materials Science and Technology, TU Wien (Technische Universität Wien), Getreidemarkt 9/308, 1060 Vienna, Austria
[b] Austrian Cluster for Tissue Regeneration, Vienna, Austria
[c] Ludwig Boltzmann Institute for Experimental and Clinical Traumatology in AUVA Trauma Research Center, Vienna, Austria
[d] University Clinic of Dentistry, Medical University of Vienna, Vienna, Austria

ARTICLE INFO

Article history:
Received 20 July 2022
Revised 10 November 2023
Accepted 1 December 2023
Available online 7 December 2023

Keywords:
Bioassembly
Spheroids
Scaffolded spheroids
Tissue engineering
Cartilage

ABSTRACT

Due to the capability of cell spheroids (SPH) to assemble into large high cell density constructs, their use as building blocks attracted a lot of attention in the field of biofabrication. Nevertheless, upon maturation, the composition along with the size of such building blocks change, affecting their fusiogenic ability to form a cohesive tissue construct of controllable size. This natural phenomenon remains a limitation for the standardization of spheroid-based therapies in the clinical setting.

We recently showed that scaffolded spheroids (S-SPH) can be produced by forming spheroids directly within porous PCL-based microscaffolds fabricated using multiphoton lithography (MPL). In this new study, we compare the bioassembly potential of conventional SPHs versus S-SPHs depending on their degree of maturation. Doublets of both types of building blocks were cultured and their fusiogenicity was compared by measuring the intersphere angle, the length of the fusing spheroid pairs (referred to as doublet length) as well as their spreading behaviour. Finally, the possibility to fabricate macro-sized tissue constructs (i.e. cartilage-like) from both chondrogenic S-SPHs and SPHs was analyzed.

This study revealed that, in contrast to conventional SPHs, S-SPHs exhibit robust and stable fusiogenicity, independently from their degree of maturation. In order to understand this behavior, we further analyze the intersection area of doublets, looking at the kinetic of cell migration and at the mechanical stability of the formed tissue using dissection measurements. Our findings indicate that the presence of microscaffolds enhances the ability of spheroids to be used as building blocks for bottom-up tissue engineering, which is an important advantage compared to conventional spheroid-based therapy approaches.

Statement of significance

The approach of using SPHs as building blocks for bottom-up tissue engineering offers a variety of advantages. At the same time the self-assembly of large tissues remains challenging due to several intrinsic properties of SPHs, such as for instance the shrinkage of tissues assembled from SPHs, or the reduced fusiogenicity commonly observed with mature SPHs. In this work, we demonstrate the capability of scaffolded spheroids (S-SPH) to fuse and recreate cartilage-like tissue constructs despite their advanced maturation stage. In this regard, the presence of microscaffolds compensates for some of the intrinsic limitations of SPHs and can help to overcome current limitations of spheroid-based tissue engineering.

1. Introduction

Biofabrication of tissues and organs using spheroids (SPHs), also referred to as microtissues, was proposed as a promising technological route leveraging some developmental biology aspects. In addition to the self-assembly capability of SPHs, it was noted

* Corresponding authors.
E-mail addresses: Olivier.Guillaume@tuwien.ac.at (O. Guillaume), Aleksandr.Ovsianikov@tuwien.ac.at (A. Ovsianikov).
[1] Equally contributed first authors.

https://doi.org/10.1016/j.actbio.2023.12.001

that they represent building blocks suitable for industrial scale robotic and automated biofabrication. In fact, the first functional bioprinted organ was fabricated, i.e. vascularized mouse thyroid gland, using spheroids, leading to a long-awaited breakthrough in the field of bioprinting [1]. Further reports have recently addressed the possibility of using SPHs for cartilage tissue engineering [2–5]. When placed in close contact, multiple SPHs can fuse and form a cohesive construct. Nevertheless, upon self-assembly, tissue constructs fabricated from multiple SPHs undergo compaction and consequently drastic volume loss. This natural phenomenon limits the stability of tissue constructs engineered using scaffold-free approaches and cuts short the versatility to biofabricate tissues with controlled 3D architectures. Mironov et al., proposed to account for this compaction, indicated by the "coefficient of tissue retraction" and the associated geometrical reconfiguration experienced by the single SPHs as well as by the produced tissue construct, in the original CAD model [6]. This approach was validated experimentally on basic tube-like structures mimicking vascular rings. Nevertheless, this significantly complicates the workflow: as first, this volumetric reduction is not only the result of the tissue compaction, but also of the release of cells surrounding the spheroid body (called non-spheroid forming (NSF) cells [7]). Secondly, the occurrence and the magnitude of both phenomena depend on many factors (e.g. cell type [7,8], cell density, SPH's degree of maturation, amount of secreted ECM [9], and others). At this stage we are not aware of any computational models integrating such a variety of factors for a predictable biofabrication of complex 3D structures.

Alternatively, rather than trying to model and account for it, one could develop technologies allowing to mitigate this compaction along with the cell detachment. Solution for such challenges can most probably be found in combining various technologies, e.g. developing hybrid biofabrication techniques, as suggested by Dalton et al. in their recent review paper [10]. Hybrid approaches have been attempted by combining cellular spheroids with micro-size objects, such as polymer fibers [11,12] or by fabricating "structured spheroids" via extrusion bioprinting followed by microfluidic emulsification [13,14]. The "Kenzan" method is another illustration where spheroids are temporarily physically constrained using microneedles. Upon spheroids aggregation and tissue maturation, the biofabricated tissue can be retrieved from this support and further used for tissue engineering and regenerative medicine (TERM) applications [15]. One can also stabilize the volume of tissue formed via self-assembly by depositing individual spheroids into pores of printed macroscaffolds. By repeated SPH deposition, Mekhileri et al. were able to engineer complex hierarchical osteochondral tissues [16]. Even though this approach is appealing for the bottom-up biofabrication of tissue, it still falls into the scaffold-based tissue engineering strategy since a "fitting" scaffold is required. In contrast to initial SPHs, the resulting constructs cannot be employed anymore as modular building block since the bioassembly potential is lost.

A synergetic tissue engineering strategy, combining the advantages of scaffold-free and scaffold-based approaches, referred to as the third tissue engineering strategy, can counter this limitation [17]. This strategy relies on producing individual SPHs directly within specialized microscaffolds, to be used as building blocks [18], referred to as scaffolded spheroids (S-SPHs). This approach is promising since important biological functions of stem cell SPHs, such as the possibility to self-assemble and to differentiate towards chondrogenic, osteogenic [18] or even adipogenic lineages [19], are maintained. We also observed that cell retention within the SPHs was improved by the presence of microscaffolds, acting as a physical cage for the agglomerated cells [18].

Nevertheless, to be able to use SPHs to reconstruct 3D organs, it is important to assess how this fusiogenicity evolves over time of culture. Indeed, it was reported that pre-cultured SPHs exhibit reduced capability to self-assemble [20,21], which limits the scope of the scaffold-free strategy. As pointed out in our previous publication [18], we observed a looser cell packing within the scaffolded spheroids, compared to spheroids (without scaffold). This aspect of loose cell packing was (among other aspects) associated with faster fusion of cellular spheroids in the work of Kosheleva et al. [22]. Therefore, we hypothesized that matured or differentiated S-SPHs show enhanced bioassembly properties compared to spheroids. The scope of this publication is to provide insight into the fusiogenicity potential of S-SPHs, compared to conventional spheroids. Our *in vitro* data suggests that the presence of the microscaffold within S-SPHs does not impair the bioassembly of doublet units when put in contact to each other. In addition, we demonstrated that, both the individual S-SPHs and the resulting bioassembled tissue constructs resulting from multiple S-SPHs show a significant lower degree of compaction, compared to SPHs independently of their degree of maturation. Finally, we proved through multiple experiments that S-SPHs exhibit a similar chondrogenesis potential compared to SPH, but possess a better fusiogenicity capacity. The chondrogenic S-SPHś cells cannot only migrate faster compared to SPH's cells, but can form a mechanically more stable tissue at the intersection between those building blocks.

In this work we demonstrate the suitability of the third strategy in tissue engineering for the biofabrication of a mature tissue construct (here cartilage-like tissue). The described method follows the bottom-up approach, using bioassembly of multiple differentiated S-SPHs as building blocks.

2. Materials and methods

2.1. Fabrication of microscaffolds

The microscaffolds were produced by two-photon polymerization (2PP) as described previously [18]. Briefly, the photosensitive PCL-based resin (DEGRAD INX) was obtained from BIO INX (Ghent, Belgium) and 0.5 wt% M2CMK was used as a photoinitiator [23]. Photo-crosslinking of the resin was performed using a femtosecond-pulsed laser (MaiTai eHP DeepSee, Spectra-Physics) operated at a wavelength of 800 nm, a repetition rate of 80 MHz and a pulse duration of 70 fs after the microscope objective (UPlanSApo, 10x/0.4 NA, Olympus, Japan). Following printing parameters, were used to fabricate 5000 microscaffolds in 24 h (equal to roughly 208 microscaffolds per hour) by aligning 3 × 3 (in total 9) microscaffolds per field of view: line/ layer spacing= 1.3 µm/ 1.85 µm, scan speed= 600 mm/s, laser power= 115 mW. Think3D software (UpNano GmbH, Vienna, Austria) was used to process the 3D files and control the hardware. The produced microscaffolds have a fullerene geometry, with a diameter of 350 µm and struts size of 35 µm. After printing, the uncrosslinked resin was washed away in Tetrahydrofuran (THF, Sigma-Aldrich, USA) and the remaining microscaffolds were sterilized and stored in 1-Propanol (Carl Roth GmbH+ Co. KG, Germany) until further use.

2.2. Cell culture and spheroid formation

Immortalized human adipose-derived mesenchymal stem cells (hASC/TERT1) (Evercyte, Austria), without and with green-fluorescent protein (GFP)-label, were used throughout the experiments. The hASC/TERT1 were retrovirally infected with GFP following the protocol by Knezevic et al. [24], whereas both stem cell lines were expanded using EGM-2 BulletKit™ medium (Lonza, Switzerland) supplemented with 10 % (v/v) newborn calf serum (NBCS) (Gibco, New Zealand) and maintained at standard culturing conditions (37 °C, 5 % CO_2, humidified atmosphere). 2 µL

of hASCs suspension (containing 5000 cells, passages 6–7) were seeded manually into each well of an agarose mold containing one microscaffold each (for S-SPH group) or none for normal spheroid group (SPH) and let to form spheroids for 2 days. Once the S-SPHs and SPHs were formed as described before, they were either directly used for the next assays (maturation week 0), transferred in DMEM-HG medium supplemented with 10 % NBCS and 1 % P/S for further maturation (for either one or two weeks) or differentiated towards the chondrogenic lineage as described in 2.3.

2.3. Chondrogenic differentiation of SPHs and S-SPHs

After spheroid formation (with and without scaffold as described in 2.2), the medium was changed to chondrogenic medium (CM) for up to 28 days, in order to induce differentiation. CM consisted of DMEM-HG supplemented with 1 % (v/v) Insulin-Transferrin-Selenium Supplement (Gibco, UK), 1 % (v/v) of P/S, 1 % (v/v) 1 M HEPES buffer (Mediatech, VA, USA), 0.1 mg/mL sodium pyruvate, 50 µg/mL l-proline, 50 µg/mL ascorbic acid 2-phosphate, 100 nM dexamethasone, 10 ng/mL of human transforming growth factor β3 (Peprotech, NY, USA) and human bone morphogenic protein 6 (R&D, MN, USA). Medium changes were carried out three times a week, while human transforming growth factor β3, human bone morphogenic protein 6 and ascorbic acid 2-phosphate were added fresh upon each medium change.

2.4. Analysis of chondrogenic differentiated units (SPH and S-SPHs)

Successful differentiation was verified by quantitative reverse transcription polymerase chain reaction (RT-qPCR) analysis of chondrogenic genes (ACAN, SOX9, COL2A1, COL10A1), as well as quantification of sulfated Glycosaminoglycan/ DNA (GAG/DNA) content of single units as described below.

For quantification of the GAG/DNA content three samples of each group (SPH and S-SPH) were collected and pooled on the first day of medium change to CM (= day 0), and on day 7, 14, 21 and 28. Pooled samples were washed three times in PBS. Subsequently, samples were prepared for DNA quantification as described in 2.8, and the DNA content was measured using the Quant-iT PicoGreen assay (Thermofisher, USA). GAG content of each sample was measured (n = 3 per group and time point) using the dimethylmethylene blue dye-binding assay (DMMB, Blyscan, Biocolor Ltd., United Kingdom), and chondroitin sulphate as standards. GAG content of each sample was normalized to the measured DNA content to receive the desired GAG/DNA ratio (n = 3 per group and time point).

For gene analysis, 10 samples per condition (SPH and S-SPHs) were pooled on each day of analysis (day 0, 7, 14, 21 and 28), washed three times in PBS and lysed in 0.5 mL QIAzol Lysis Buffer (Qiagen, Netherlands). Total RNA was extracted using RNeasy Mini Kit (Qiagen, Netherlands) according to manufacturerś protocol, subsequently the RNA concentration was measured using the microplate reader Synergy H1 (BioTek, USA). RNA concertation was diluted to result in 100 ng/ reaction for the cDNA synthesis (=reverse transcription) using the All-In-One 5x RT MasterMix (Applied Biological Materials (ABM), Canada). cDNA was diluted 1:5 in nuclease-free water and RT-qPCR was conducted using the primers listed Table 1. For RT-qPCR following program was applied using the CFX Connect Real-Time PCR Detection System (Bio-Rad, USA): 3 min at 95 °C, followed by 40 cycles of Denaturation at 95 °C for 10 s and annealing/extension at 60 °C for 30 s. The gene expression was normalized to the housekeeping gene (HPRT1), while samples collected on day 0 were used to calculate the relative gene expression. For low expressed genes, a cut-off CT-value of 40 was defined (in case of SOX 9 for day 0, and ACAN for day 0 and 7) as previously described by Žigon-Branc et al. [25] (n = 3 per group and time point).

2.5. Study of the fusion kinetics

The aim of the experiment was to assess, the speed and quality of the doublet's fusion using SPHs compared to S-SPHs, and to which degree it depends on their pre-culture time (0, 1 or 2 weeks, referred to as maturation). To allow for fusion, two S-SPHs or two SPHs, were transferred from the agarose mold to wells of U-bottom 96 well plate, coated with hydrophobic coating Lipidure® (Amsbio, USA) beforehand to prevent cells from attaching to the plastic. At regular time-points, images of the doublets were taken using a light microscope and processed using Fiji [26]. The fusion kinetics was evaluated by quantifying the intersphere angle between the doublets and the doublet length over 8 days of culture (n = 6 to 11 per condition, see Fig. 1). A fusion angle of 180° was considered as complete fusion, as the two fused units are not discriminable anymore at this time point. Therefore, the fusion experiments were stopped as soon as a fusion angle of 180° was reached (complete fusion).

2.6. Assessment of the spreading kinetics

The aim of this experiment was to determine if the presence of microscaffolds influences the spheroids' ability to attach and to spread once in contact with tissue culture plastic. For this experiment, SPH and S-SPHs were prepared using GFP-labelled hASC and individually transferred to a flat-bottom tissue culture treated 96 well plates after maturation (at maturation week 0, 1 and 2). Using a LSM 700 (Zeiss, Germany), fluorescent images of the spreading building blocks were taken regularly over 7 days, and the images were processed using Fiji [26] to analyse the evolution of the spreading areas. For this quantification, images were first transformed into a 32-bit image, followed by manually setting/defining a segmentation threshold. The area was finally measured after setting the outline fitting the spreading area (Fig. 2A), n = 12 per condition.

2.7. Bottom-up bioassembly of defined defects in vitro

At a later stage (e.g. translation to clinics and *in vivo* experiments), the main goal of any bottom-up TERM approach is to fill up a defined defect of known volume and be able to have control over this aspect. To this end, here a custom-made mold (resembling) the TU Wien logo as a complex-shaped defect was created on a SLA 3D printer (Form 2, Formlabs, MA, USA) using a heat-resistant resin (High Temp Resin, Formlabs, MA, USA). Custom-made TU-logo-shaped molds were produced using 3 wt% agarose (Sigma-Aldrich, USA) in a glass-bottom cell culture dish (ibidi GmbH, Germany) by using the 3D-printed model as counterpart during the hardening of the Agarose form. After complete hardening the 3D-printed counterpart was removed from the mold, and the void was filled with 2 mL EGM-2 BulletKit™ medium (Lonza, Switzerland) supplemented with 10 % (v/v) newborn calf serum (NBCS) (Gibco, New Zealand), as well as 1% P/S and incubated at standard culturing conditions (37 °C, 5 % CO_2, humidified atmosphere) overnight. The amount of S-SPHs to fill up the defined volume was calculated to be 180 units, by assuming a packing density of 74 % (as face-centered-cubic filling was assumed). The defect was filled up with GFP-labelled S-SPHs or SPHs respectively and incubated for 6 h at 37 °C, 5 % CO_2, humidified atmosphere. Subsequently, z-stack analysis of each sample was done using a confocal microscope (LSM 800, Zeiss, Germany). Each layer of the resulting z-stack was automatically thresholded (background

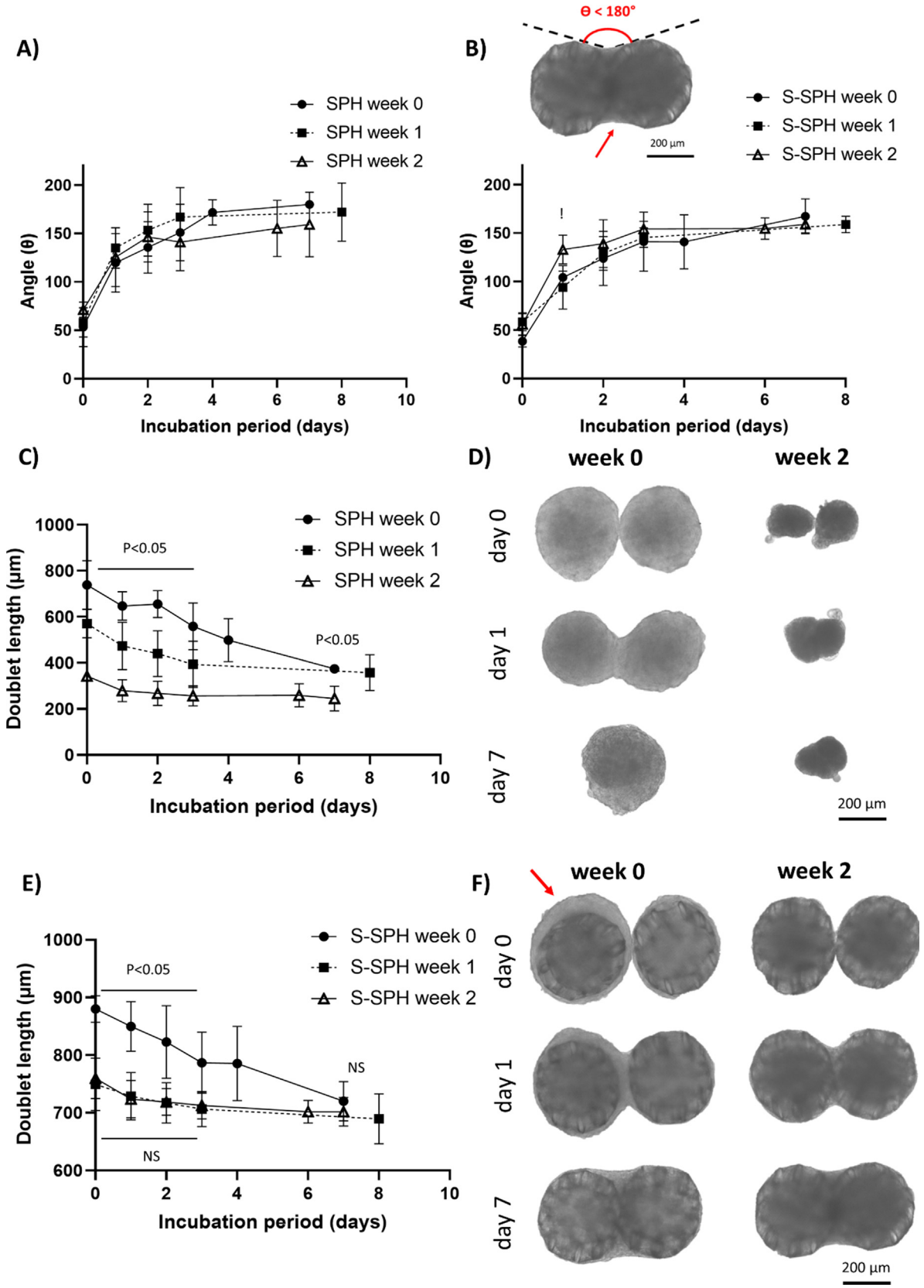

Fig. 1. SPHs suffer from greater shrinkage compared to S-SPHs for all three tested degrees of maturation. Fusion kinetics of SPHs and S-SPHs were assessed by measuring the intersphere angle for up to 8 days of doublet incubation, on samples with different degrees of maturation (week 0, 1 and 2). Intersphere angle measurement was performed until a value of 180° was reached for SPHs (A) compared to S-SPHs (B). ! denotes significance between S-SPH week 0 and week 2, with a higher angle for week 2. A red arrow highlights necking of S-SPHs doublets (B). Doublet length was assessed over 8 days on samples of different maturation times, and imaged using bright field microscopy for SPHs (C and D) and for S-SPHs (E and F). Differences between the three degrees of maturation are all significant for the SPH group. For S-SPHs, statistically significance was found only when comparing week 1 and 2 with week 0. A thick mass layer of cells is visible just after the formation of the S-SPH, outside the microscaffold (pointed by the red arrow).

Table 1
Primers used for RT-qPCR analysis of chondrogenic genes, all primers were purchased from Bio-Rad, USA.

Gene (abbreviation)	Gene name	Manufacturer, assay ID
SOX9	SRY (sex determining region Y)-box 9	BioRad, qHsaCED0021217
COL2A1	Collagen type II, alpha 1	BioRad, qHsaCED0001057
COL10A1	Collagen type X, alpha 1	BioRad, qHsaCID0007356
ACAN	Aggrecan	BioRad, qHsaCID0008122
HPRT1	hypoxanthine phosphoribosyltransferase 1	BioRad, qHsaCID0016375

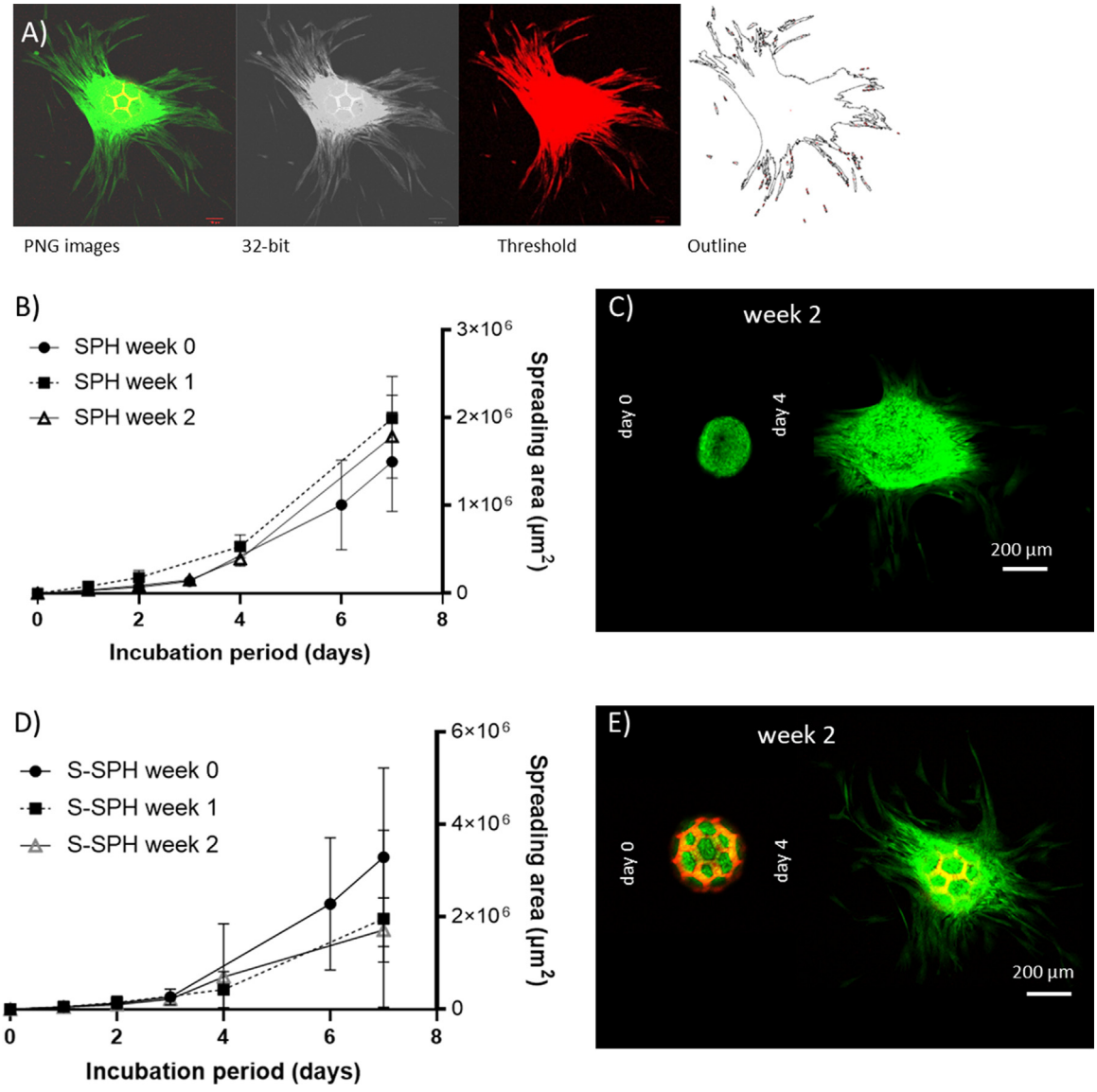

Fig. 2. The ability of the spheroids to spread is not inhibited by the presence of the microscaffolds. Illustration of the workflow undertaken to analyse the spreading of the cells using Fiji software (A). The spreading areas were analysed over 7 days of incubation for samples of different degrees of maturation (B and D for SPH and S-SPH). Fluorescent images are shown for 2-weeks old SPH and S-SPH, at day 0 and day 4 exhibiting advanced spreading (C and E for SPH and S-SPH). At day 7 of incubation, differences between SPH and S-SPH, and between week 0, 1 and 2 are statistically not significant.

correction) to measure the area occupied by GFP-labelled cells using Fiji [26]. The measured area was multiplied by the height of each layer (35 µm) to result in the volume of the filled space. The resulting volume was normalized to the calculated total volume (=100 %) of the mold and the comparison between S-SPH and SPH group is depicted (n = 1/group).

2.8. Cell migration from S-SPH to empty microscaffolds

The goal of this experiment was to investigate the capacity of empty microscaffolds to be colonized by the cells from the adjacent S-SPHs. This experiment required the formation of S-SPHs, which were subsequently cultured together with different num-

bers of empty microscaffolds (ratios ranging from 1:1 up to 1:8, Group C). As control groups, SPHs only (Group A) and (cell-laden) S-SPH only (Group B), were used (with similar final quantity of building blocks as for the experimental group, i.e. 2–9 SPHs/S-SPHs cultured together). The SPHs and S-SPHs used for this experiment were prepared as mentioned in 2.2. Morphological changes including the bioassembly and the colonization of the empty microscaffolds were imaged over 9 days of culture (n = 5 to 8 per condition). To determine the final number of cells in the 9-days old tissue constructs, DNA quantification was performed for samples from all three groups. Firstly, this required samples to be digested with 125 µg/mL papain in 0.1 M sodium acetate, 10 mM l-cysteine-HCl, 50 mM EDTA (all from Sigma-Aldrich) adjusted pH 6.0 and incubated at 55 °C under constant shaking for 18 h. DNA content of each sample was quantified using the Quant-iT PicoGreen assay (Thermofisher, USA) (n = 5 to 8 per condition). Finally, the viability of the hASCs of one tissue construct of Group C (ratio 1:6) was assessed after 15-day culture using Live/Dead® assay (Invitrogen, Thermofisher), based on 0.2 µM calcein-AM (live stain) and 0.6 µM propidium iodide (dead stain), using a LSM 700 (Zeiss, Germany).

2.9. Cell migration and fusion study on doublets of chondrogenic differentiated units

In order to systematically test and analyze the fusion behavior of mature SPHs versus S-SPHs, the following experiments were conducted. After successful chondrogenic differentiation for 28 days, as described in 2.3, the kinetic of cell migration in doublets of chondrogenic SPHs or S-SPHs respectively was characterized. To allow for cell tracking via LSM imaging, only one of the two spheroid units was composed of GFP-labelled cells. One chondrogenic (unlabelled) hASCs sample (either S-SPH or SPH) and one chondrogenic GFP-labelled hASC sample were pipetted into a well of a U-shaped well plate previously coated with hydrophobic coating Lipidure® (Amsbio, USA) to prevent cells from attaching to the cell culture plastic. Plates were tapped and pivoted in order to guarantee close proximity of samples in the well, which was verified under the light microscope on day 0. Over the course of 15 days, the fusion process was monitored in regular intervals by LSM-z-stack imaging. The resulting imaging data was post-processed using a custom-written macro for Fiji [26], which was made available online [27]. To define the region of interest (ROI) the macro was applied to z-stack LSM images taken on day 0, and included following functionality: generation of maximum intensity projection of the measured z-stacks (including background correction), followed by channel separation. Furthermore, a blurring filter and masking of the image based on the fluorescent signal was conducted. Subsequently, a circle was fitted based on the outline of the masked region, and the left most pixel of the circle was defined as center of the fusion area. This applies, since in all images the GFP-labelled SPH/S-SPHs was present on the right side of the fusion area. In a last step the macro automatically defined three ROIs, the intersection region around the identified center of the fusion area, and two neighboring regions (with defined area as well) covering both sides of the fusion area (region of labelled/unlabelled SPH/S-SPHs) as depicted in Fig. 4A. Applying the defined ROIs (from day 0) of each sample to the corresponding later time points and measuring the mean intensity fluorescence in each of the defined ROIs allowed quantifying the cell migration from the GFP-labelled SPH/S-SPH into the intersection area and subsequently the neighboring unit using the described macro. The background corrected mean fluorescence intensity of each ROI was normalized to the signal of the GFP-labelled sample for each image (referred to as right ROI). The progression over culture time (up to day 15) is depicted in Fig. 4B. Furthermore, the diameter of the fusion area was measured using Fiji [26] between day 1 and day 15 of fusion (Fig. 4E). Number of units per condition n = 3–6 (depending on the time point). All images were taken on LSM 800 (Zeiss, Germany).

2.10. Mechanical characterization of fused doublets

Chondrogenic doublets, prepared as described in 2.6, were transferred into the PBS-filled reservoir of the MicroTester (CellScale, Canada) on day 3 of the fusion process. The samples were positioned under the beam (0.3048 mm, with no platen mounted) in order to compress the fusion area until complete separation of the doublets. The measured maximum force (at break) F_{max} was used to calculate the shear stress τ_{max} applied [28] to separate the two fusing units. The formula for the shear stress calculation is depicted in Fig. 4C along with an illustration of the used setup. The fusion areas A (required to calculate the shear stresses) were calculated from the fusion area diameters (as circular fusion area was assumed) (n = 4 per condition).

2.11. Bottom-up assembly of mature cartilage-like tissue

We tested the possibility to recreate a cartilage-like tissue *in vitro* by assembly of 500 SPH or S-SPHs, which were differentiated towards a chondrogenic lineage for three weeks as previously described in section 2.3. Custom-made cylindrical 3 wt% agarose molds (Sigma-Aldrich, USA) with Ø1.4 mm, housed in a 15 mL falcon tube were filled up with 500 S-SPHs or SPH. To guarantee close proximity to each other, the falcon tube was centrifuged at 300 g for 3 min. For the merging period of 7 days (inside the mold) DMEM-HG medium supplemented with 10 % NBCS and 1 % P/S was used and daily medium changes were performed. After the merging period the samples were extracted from the mold by cutting the mold open using a scalpel. The resulting plugs were washed in PBS (Sigma-Aldrich, USA) and subsequently fixed in 4 % formaldehyde (Roti Histofix 4 %, Roth, Germany) for 12 h at 4 °C. The quality of the produced cartilage tissue constructs was assessed using histology as followed. After rinsing the plugs with PBS and dehydration with increasing ethanol solutions, starting with 50 % ethanol, the samples were immersed in xylene and finally wax-embedded. The plugs were then cut in 4 µm thin sections and dried overnight in a 37 °C incubator. After deparaffinising the sections, they were re-hydrated and then stained with 0.1 % Alcian blue solution at pH 2.5 (Merck, Germany) for 30 min at room temperature to visualize Glycosaminoglycan (GAG) deposition. Samples were counterstained with Mayer's Haemalaun (Roth, Germany), dehydrated and mounted with Consul Mount (Thermofisher, USA). Another section from each sample was stained with PicroSirius Red to visualize collagen. First the samples were stained with Weigert's Iron Haematoxylin (Roth, Germany) for nuclei and after rinsing in dH_2O stained for one hour in PicroSirius Red solution: 0.1 % DirectRed 80 in saturated picric acid (Merck, Germany). After that, the samples were rinsed in 0.5 % acidic acid solution, dehydrated and mounted with Consul Mount. Subsequently, the stained sections were imaged on an upright clinical microscope Eclipse CI (Nikon, Japan).

2.12. Statistical analyses

Statistical analysis of the presented data was performed using Prism 9 software (GraphPad Software, USA). Normal distribution of the data was verified using a Shapiro-Wilk test performed in Prism 9 software (GraphPad Software, USA). Student t-test was applied to analyze the significance of differences between two experimental groups (with $p < 0.05$). Data presented are means ± standard deviation (SD) unless stated otherwise.

3. Results

3.1. Influence of the microscaffold on the fusiogenicity and compaction of spheroids

A prerequisite for the third tissue engineering strategy, based on the use of multiple S-SPHs as building blocks, is the possibility for them to bioassemble into larger cohesive constructs. This property relies on fusion, which can be assessed by measuring the intersphere angle on doublets during culture (Fig. 1). Following the incubation of doublets of SPHs (Fig. 1A), their rapid fusion was observed, until they form a single agglomerate, with an angle of 180° within three to four days for freshly prepared or for 1-week old SPHs. With higher degree of maturation (i.e. 2-weeks old SPH), this 180° intersphere angle was reached after longer incubation time, i.e. 6 days (Fig. 1A). For the S-SPHs, the kinetic of fusion was not negatively altered by the spheroid maturity, and all three maturation stages reached the maximal intersphere angle (i.e. 150°) after 3 to 5 days (Fig. 1B). The presence of the microscaffold does not restrict their fusion, but prevents the doublets from fusing into a single indistinguishable spheroid, as it is observed for SPH group. The resulting S-SPH doublets exhibit a rather oblong-shape, with a slight "necking" at the contact area, corresponding to an intersphere angle between 150 and 160° (Fig. 1B).

We analysed the evolution of doublet length over 7–8 days of culture, based on the degree of maturation of SPHs and S-SPHs, starting from the doublet length recorded just after the incubation of the doublet (at day 0). It has to be noted that the initial doublet length is smaller for more mature SPHs since they are also smaller individually. For instance, at day 1 of the fusion experiment, freshly prepared SPHs (maturation week 0) have a doublet length of ~740 µm, while it is only 570 and 345 µm for samples from the 1-week and 2-weeks maturation group respectively (Fig. 1C). Those morphological changes and the compaction phenomenon were monitored using optical microscopy (Fig. 1D), with week 0 SPHs being significantly larger than week 2 group. Secondly, the length of the doublets significantly decreases with prolonged incubation time. The degree of this compaction correlated to the maturation stage, with younger SPHs experiencing more reduction than 1 or 2-weeks old ones. The resulting merged tissue construct at day 7 is consequently smaller when using more matured SPHs compared to "younger" SPHs.

Subsequently, we compared the doublet length obtained from SPH with the one from S-SPH (Fig. 1E and F). It has to be noted, that although the same number of cells (5000 cells/unit) was used for both tested groups (SPH and S-SPH) the initial measured doublet length on day 0, was already larger for S-SPHs compared to SPHs (~880 µm for S-SPH compared to ~740 µm for SPH). This can be explained by the presence of the microscaffolds that results in a mass of cells excluded from the core of the microscaffold and ending up outside the latter (pointed by the red arrow Fig. 1F). The volume of the scaffold accounts for approximately 33 % of the additional cell mass, on day 0 S-SPHs. As the S-SPHs matured, this mass of cells was no longer visible around the microscaffold. Based on the previous observations we conclude that this is a result of the compaction process, which stops at the microscaffolds' border for the S-SPH group [18]. When measuring the doublet length of S-SPHs, there is a significant reduction for S-SPHs freshly formed (week 0), specifically due to the retraction of this mass of cells overtime (day 0 = 880 µm and after 7 days = 720 µm). Conducting this fusion experiment with 1- or 2-week mature S-SPHs results in different behaviour. Indeed, S-SPHs show a smaller range of doublet size reduction compared to SPHs. The initial measured doublet length for S-SPHs is ~760 µm while after 8 days the doublet length decreased slightly to ~700 µm. This experiment further revealed that this mass of cells initially surrounding the microscaffold is not a prerequisite for the fusiogenicity of S-SPH, since more mature S-SPHs without this cell mass are still able to fuse. Therefore, decreasing the number of cells that are seeded onto each scaffold can help to circumvent the formation of this initial additional cell layer from the beginning. The doublet size reduction observed for S-SPHs is significantly different compared to what was described previously for SPHs. The same data presented after normalizing to the double length registered at day 0 further supports this conclusion (SD 1). There is a strong reduction of doublet length of SPHs depending on both, the time of culture and their degree of maturation, with a reduction of up to 50 % for young and of 30 % for 2-weeks old SPHs (SD 1A). Using S-SPHs enables the stabilization of the doublet length, with a reduction of less than 10 % for 1-week and 2-weeks old building blocks (SD 1B). A later maturation time point was tested (week 3) on both groups to verify the stability of the bioassembled doublet (SD 1C). The similarity of the doublet length for the 3 maturation time points (week 1, 2 and 3) with no residual mass of cells for the S-SPH group validated the previous statement. Differences between SPHs and S-SPHs were significant for all the maturation time points. The size homogeneity of the bioassembled tissue resulting from S-SPHs is reflected by the lower STD values compared to the SPH group (SD 1C). Therefore, the microscaffolds not only support fusion, but compared to SPH, also allow to control and predict the volume of the bioassembled tissue engineering constructs.

For multicellular building blocks to be used in tissue engineering, one must not only ensure that they can fuse into one single tissue-construct, but that they can also interact with their surrounding and attach to it. This aspect can be assessed *in vitro* by characterizing the spreading behaviour of single building blocks on tissue culture plastics. In our experiment, we compared the spreading behaviour of SPHs and S-SPHs prepared from GPF-labelled hASCs, and recorded the fluorescence signal using a laser scanning microscopy system. The workflow together with the image analysis is shown Fig. 2A.

SPHs placed onto tissue culture plastic rapidly attached to it and enabled cells to spread, from an initial area of 50-100 $\times$ 10^3 µm^2 reaching 1.5–2.0 $\times$ 10^6 µm^2 after only 7 days. The spreading kinetics does not seem to be dependent on the degree of maturation, as the evolution was similar for SPH week 0, 1 and 2 (Fig. 2B). From the initial location of the spheroid at day 0, the area formed by adhering cells starting from the SPH, elongated in x- and y-direction due to the migration and proliferation of the hASC from the SPH body (Fig. 2C).

S-SPHs exhibit similar spreading evolution, with a final spreading area similar to the one obtained for the SPH group. Freshly prepared S-SPHs resulted in a final spreading area (after 7 days) that appeared larger compared to samples with a higher degree of maturation (1 and 2 weeks), which can be attributed to the additional cell mass present on early time point S-SPHs as discussed above (Fig. 2D and E). Anyhow, statistical analyses performed at the last day of spreading experiment (day 7) revealed no significant differences between SPH and S-SPH group, and between the three maturation stages for both groups.

After having shown that S-SPHs exhibit good fusiogenic and spreading behaviour, and that the tissue-construct resulting from the bioassembly of doublets of S-SPHs is better controllable in size than using SPHs, we assessed the potential of S-SPHs to fill up a complex shaped defect of defined volume. The amount of units needed to fill up the defect was calculated to be 180, therefore the cavity with the shape of "TU Wien" logo was filled with 180 GFP-labelled S-SPHs or with a similar number of SPHs (Fig. 3A). This experiment revealed that indeed the enhanced control over compaction in case of the S-SPHs helps to fill up the defined volume very precisely compared to the SPHs group (filled up volume compared to the total volume: 89 % for SPHs to 103 % for S-SPHs).

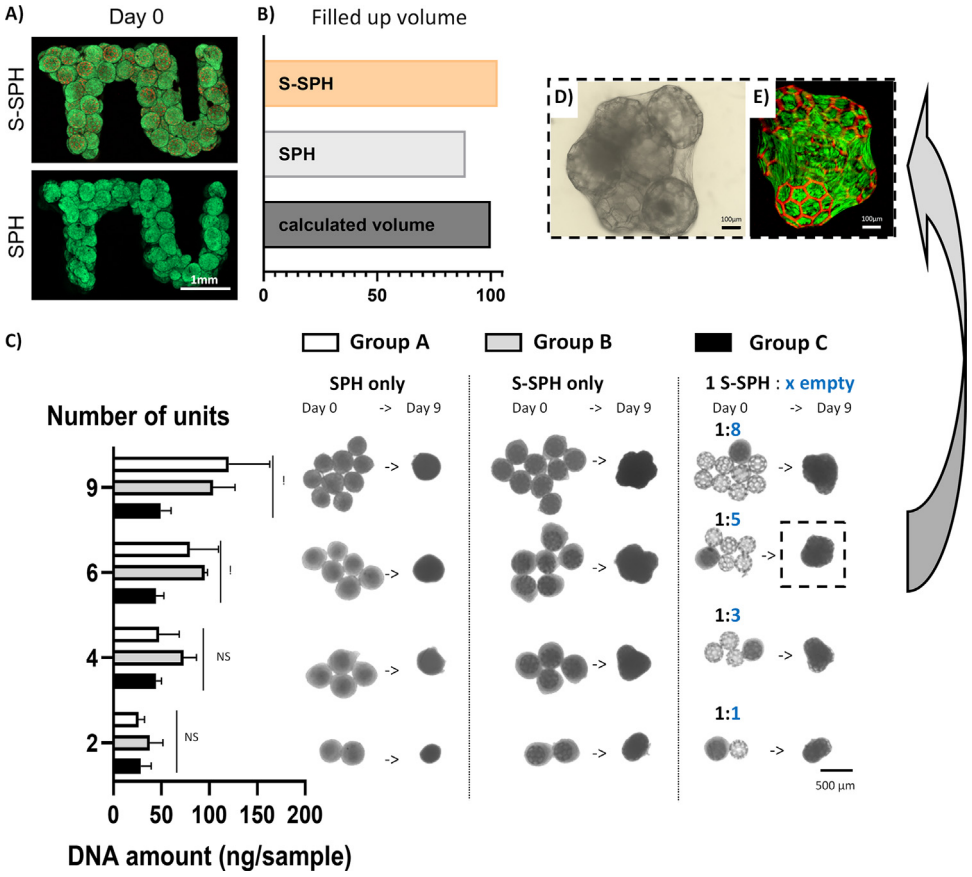

Fig. 3. Bioassembly of scaffolded spheroids produces stable tissue constructs and offers the opportunity to be combined with empty scaffolds.
TU-logo construct consisting of 180 units (SPH versus S-SPH) used to mimic a complex- shape defect (A) and verification of filled up volume after seeding, normalized to "defect" volume (B). The degree of cellularity of multiple merged units (2, 4, 6 or 9) was assessed by DNA quantification and imaged using bright field microscopy, of SPH only (Group A), S-SPHs only (Group B), and a combination of one S-SPH and empty microscaffolds (Group C) of various ratios (C). ! denotes significance between Group C and Groups A-B, whereas non-significance is abbreviated "NS". Microscopic observations of one sample of Group C, ratio 1:5 (D) and its viability assessment (Live/Dead staining, E) after 15 days of culture.

While for the SPH group roughly 11 % of the defect remained unoccupied, the S-SPH group showed complete filling of slightly above 100 % (most likely due to the fact that the volume is not confined from the top, allowing "overfilling" of the defect), as depicted in Fig. 3B.

Having shown that the S-SPH offers the possibility to bioassemble into a tissue with more controllable size than conventional spheroids do, we then explored the possibility to combine cell loaded S-SPHs with cell-free S-SPHs (empty scaffolds). For that, the same number of SPHs and S-SPHs (from 2 to 9) was incubated together over 9 days, but their composition varied. Controls based on SPH and S-SPH only were analysed as Group A and B respectively. In order to assess the colonization potential of the cells from S-SPHs, a third group was tested, based on only 1 S-SPH with increasing number of empty microscaffolds (from 1 up to 8, Group C, Fig. 3C). Multiple building blocks (either based on SPH or S-SPH and microscaffolds) cultured together merge into one single tissue structure within a few days. The determination of the DNA-content after 9 days of culture revealed no statistical difference between bioassembled tissue constructs made of SPH or made of S-SPH only, as expected. For both groups, the increasing amount of building blocks resulted in tissue constructs with linearly increasing amounts of DNA (Fig. 3C). Interestingly, the same bioassembly behaviour is also observed when multiple empty microscaffolds are incubated with a single S-SPH. Even though the amount of DNA is significantly lower in this group (Group C) compared to SPH or S-SPH only (Group A and B respectively), the cells from S-SPH are able to colonize the empty microscaffolds over time of culture. This enables multiple building blocks to bioassemble into a single tissue, even when the majority of them are cell-free microscaffolds. We prolonged the culture duration for one sample of Group C with ratio S-SPH:empty microsaffolds of 1:5 for a total of 2 weeks. From the image presented in Fig. 3D, it can be seen that the cells have migrated and colonized the entire structure. A high viability of the hASCs is maintained as shown by the Live and Dead staining (Fig. 3E).

3.2. Influence of the microscaffold on the chondrogenic differentiation and on the ability of S-SPH to form cartilage-like tissues

After assessment of the fusion ability of SPHs and S-SPHs relative to their degree of maturation, we tested their fusion ability when differentiated towards a chondrogenic phenotype (which is associated with ECM deposition, known to influence the fusion ability).

We used GFP-labelled cells in a doublet experiment over 15 days of incubation (Fig. 4A), to study the cell migration via confocal laser scanning microscopy. In the intersection area, where colonization first happens, higher mean fluorescence intensities were detected for S-SPH compared to SPH for the first five days of this experiment (Fig. 4B). This feature was indicating a faster migration of the cells present in the scaffolded spheroids. For longer in-

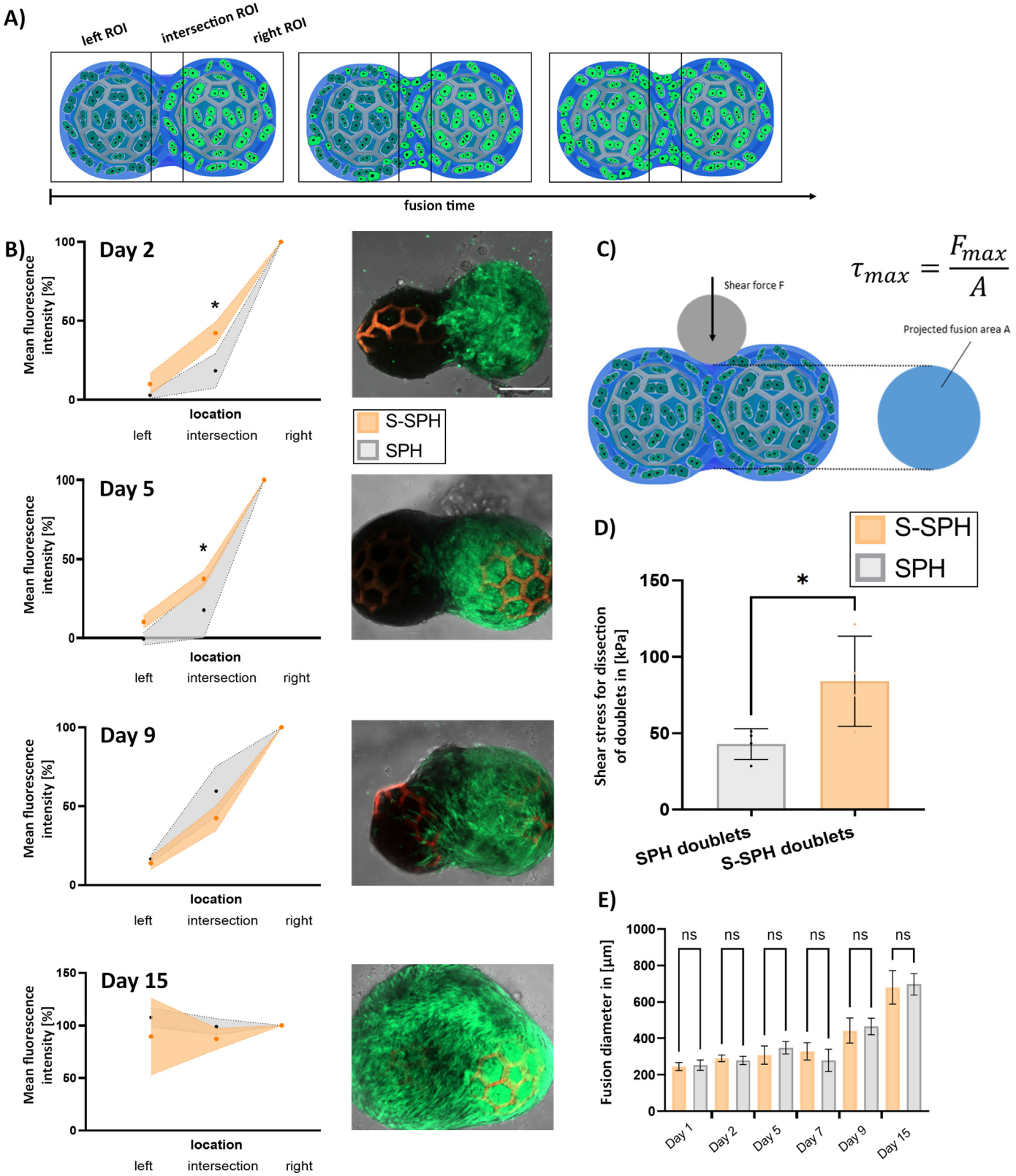

Fig. 4. Chondrogenic S-SPHs show stronger cohesion and faster migration rates compared to chondrogenic SPHs. Visualization of the workflow of cell migration experiments and cell culture progression over time including the ROI definition (A). Quantification of the mean fluorescence intensity for each ROI on day 2,5,9 and 15, * denoting significance between the two tested groups (B). Graphical representation of the dissection experiment setup performed using a MicroTester, depicting the beam that was applied to dissect two fused units. Visualization of the projected area and formula for shear stress calculations (C). Record of the maximum shear stress needed to separate two fused units, with * denoting significance between the 2 groups (D). Analysis of the fusion diameter of S-SPHs and SPH, no significant difference between both groups when compared on individual time points (E). Scale bar is 200 µm.

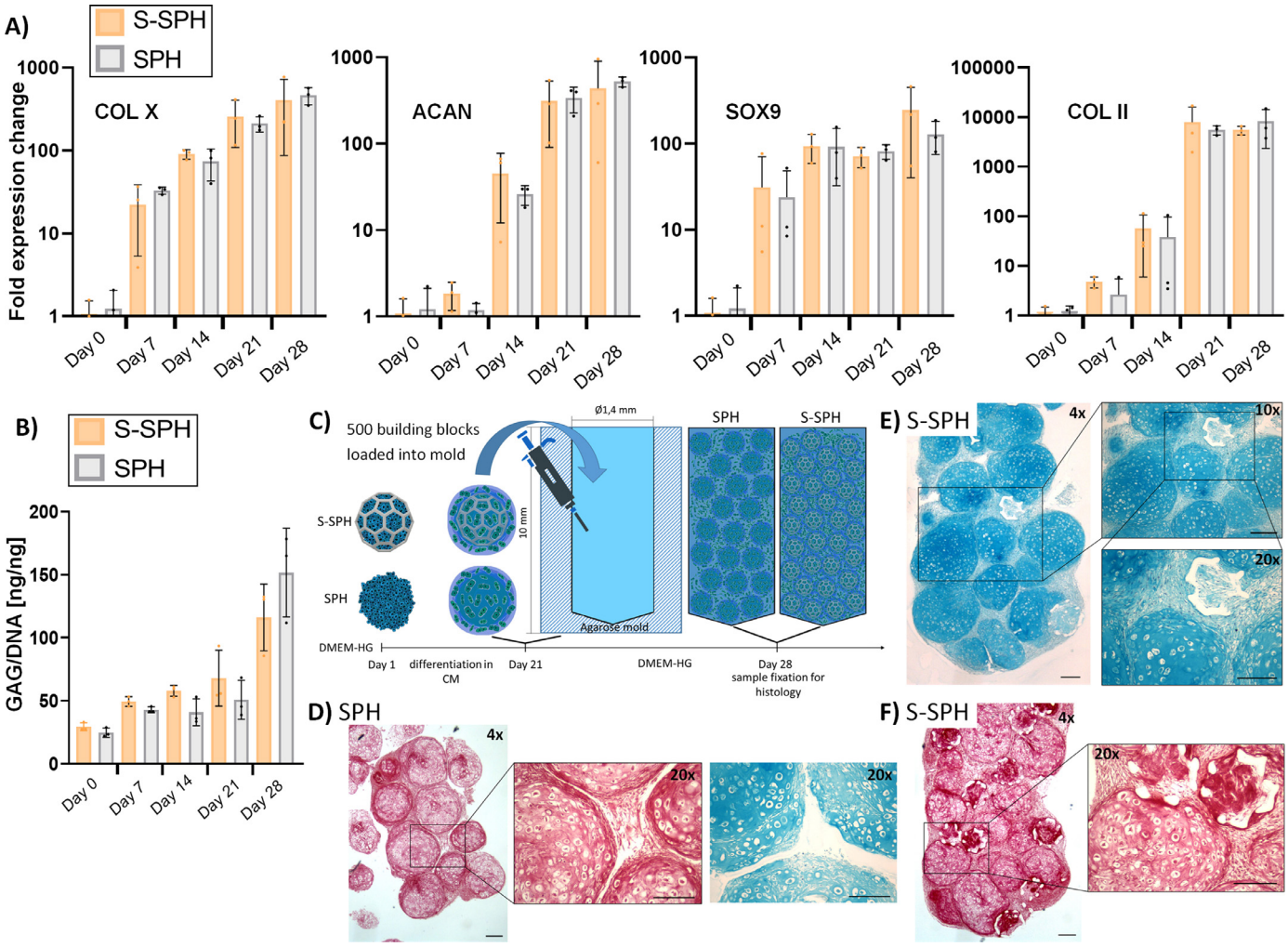

Fig. 5. Chondrogenic S-SPH can be used as building blocks for engineering cartilage-like tissue via bioassembly. Chronological evolution of the gene expression of key chondrogenic markers (A) and of GAG/DNA ratio (B) of SPHs versus S-SPHs. Depiction of the workflow used to create cartilage-like tissue via self-assembly of SPH versus S-SPH (C). PicroSirius Red and Alcian Blue histological staining of SPH (D) and S-SPH (E and F) bioassembled cartilage-like tissues. Scale bar in each figure is 200 µm. For lower magnification images a 4× objective was used, while for higher magnifications a 10×/20× objective was used. No significance was denoted comparing SPH versus S-SPH for A and B. (For interpretation of the references to color in this figure legend, the reader is referred to the web version of this article.)

cubation time, no further significant differences were registered, and the GFP-labelled cells were not only present in the intersection area but were found also in the neighbouring unit (SPH or S-SPH), indicating cell mixing between doublets at later time points for both tested groups.

After having demonstrated that the migration of cells was influenced by the presence of the microscaffold, an experiment was conducted to test if this phenomenon results in increased cohesion between S-SPH units as well. For that, we assessed the mechanical stability of the intersection area of doublets through a dissection experiment, performed on day 3 of doublet fusion, using a MicroTester (set up shown in Fig. 4C). Once more, differences between both groups were detectable, as the shear stress required to dissect a doublet of S-SPH was almost twice as high as for the SPH doublets (Fig. 4D), although the fusion diameters were similar over culturing time (Fig. 4E).

After having shown that chondrogenic S-SPHs show an increased fusionability especially in the first days of cell migration, we conducted a final experiment where we compared the possibility to use mature, chondrogenic SPHs and S-SPHs to bioassemble into a cartilage-like tissue construct. To exclude that the microscaffold influenced the differentiation process, we first analysed the gene expression and GAG synthesis over 4 weeks of differentiation. In fact, no differences were noted between SPH and S-SPH in terms of chondrogenic gene expression and GAG synthesis (Fig. 5A and B). Over the culture in CM medium, both SPH and S-SPH followed the same trend, characterized by a steady increase of all tested chondrogenesis markers (Fig. 5A). Furthermore, no significant difference of GAG content (normalized to DNA content) could be detected when comparing SPH and S-SPH on the same day of culture (Fig. 5B). After successful differentiation in CM medium, 500 building blocks of both groups (S-SPH vs. SPH) were manually transferred into custom-made agarose molds for 7 days of merging (see workflow in Fig 5C). The extracted plugs, showed an intensive GAG and collagen deposition, detectable homogenously across the entire section for both groups (Fig. 5D-F). Additionally, anatomical features resembling of cartilage, e.g. lacunae hosting chondrocytes within the deposited ECM, are clearly visible for both groups, which emphasizes the overall applicability of the utilized method.

Interestingly, while the S-SPH group resulted in one cohesive plug, the SPH-based plug was characterized by an overall less connected structure with lower mechanical stability. This was not only noticeable by the smaller size of the resulting construct but also by the presence of multiple single SPH-units that did not integrate into the plug structure (Fig. 5D). Further analysis performed using histological staining corroborated this findings. Higher magni-

fication microscopic images of PicroSirius red stained histological sections confirmed the superior merging ability of S-SPHs compared to SPHs. Indeed, for the SPH-group, numerous voids especially alongside the intersection of building blocks were clearly visible. This was not visible on the S-SPH-group, as this group was able to form one cohesive tissue construct. In this group, the voids in-between neighbouring S-SPH units were invaded and filled up by cells and ECM (Fig. 5E and F). From our histology staining, this intersection tissue between different S-SPHs is rather poor in GAG but rich in collagen. This result corroborates previous work from Lindberg et al., who observed that chondrogenic hASC-spheroids, when merged together, secreted a fibrocartilaginous-like ECM in the tissue fusion area [29]. This results further strengthen the findings already described in Fig. 4 regarding the superior stability of the S-SPH bioassembled chondrogenic doublets, compared to SPH.

4. Discussion

We have previously reported on the possibility to produce S-SPHs to be used as building blocks for the third tissue engineering strategy [18]. The present work gives insights into the evolution of the fusiogenicity of these S-SPHs upon tissue maturation. For the biofabrication of large size tissue constructs based on a bottom-up approach, it is important to verify if the presence of microscaffolds influences the bioassembly behaviour of S-SPHs. Indeed, fusion is a fundamental biological process for SPHs to be used as building blocks in tissue engineering. This fusiogenicity, enables the engineering of cohesive and large size tissue constructs with cell densities approaching those of native tissues [30]. Nevertheless, the standardization of the tissue resulting from the self-assembly approach remains extremely complicated due to 1- the impact of the degree of maturation of the single SPHs on their fusiogenicity, and 2- the substantial compaction of the final tissue-construct occurring over extended culture time

4.1. S-SPHs exhibit fusiogenicity uncoupled of their maturation

The fusiogenic potential of spheroids (SPH) is dependent on their *in vitro* preculture time (referred to as degree of maturation) as reported by several authors [20,21,31]. Older SPHs (i.e. longer preculture time) and more mature (i.e. differentiated SPHs) do not equal freshly prepared samples in their ability to self-assemble. Consequently, this degree of maturation is a decisive factor for bottom-up strategies. For instance, Nilsson et al. reported that increasing the degree of maturation of cartilaginous SPHs resulted in a significant decrease of the spreading. Similarly, the self-assembly potential of multiple SPHs grown under chondrogenic condition was also drastically reduced by 3 weeks of maturation period [31]. From our first set of experiment conducted on doublets (grown in DMEM HG supplemented with 10 % serum medium, considered to be relatively “poor” medium), we could not detect any correlation between the maturation (after 2 to even 3 weeks of *in vitro* culture) and the fusiogenicity of both the SPH and the S-SPH group. Neither the culture time, nor the presence of the microscaffold decreased the ability of building block doublets to fuse into a single body.

In the literature, an increase in ECM deposition within the SPHs and/or a rearrangement of contractile cells responsible for F-actin protein synthesis surrounding the SPHs have been suggested as probable reasons for this reduction of fusiogenicity with time [31]. Our previous study did not show any significant difference in terms of amount of protein comparing S-SPH and SPH [18], which might explain why the presence of the microscaffolds does not restrict their merging behaviour.

Nevertheless, in our second set of experiments where more mature and at the same time differentiated building blocks were produced (after 3 weeks of culture in CM condition), S-SPHs still exhibited potent fusiogenic capability and were able to bioassemble into a cohesive large size cartilage-like tissue construct. This feature was lost for SPHs cultured under identical conditions. This behaviour cannot be explained by an uncomplete chondrogenic differentiation of S-SPH compared to SPH, as we have not observed any gene expression or biochemical-related dissimilarities between those two groups. We hypothesised that the fusiogenic superiority of the differentiated S-SPHs can be explained by a different cellular behaviour on the surface of the S-SPHs compared to SPHs. In fact, more migrating cells were observed on the intersection area of doublets of S-SPH compared to SPH in the first 5 days of fusion. Cells from S-SPH migrated faster which could allow them to infiltrate the voids in between neighbouring building blocks easier or faster compared to SPHs. This hypothesis was validated when conducting the dissection experiment, where we noted higher shear stresses required to rupture the fusion area of 2 S-SPHs compared to 2 SPHs. Furthermore, after an initial faster migration of cells observed in S-SPHs during the first 5 days of fusion study, no significant differences between the two tested groups in terms of cell migration could be found. This observation leads to the conclusion that initially the presence of the microscaffold supports cell migration in the early phase of fusion, while it is not interfering in the later stage of fusion, once ECM is formed in the fusion area.

In our present work, we have shown that culturing spheroids within microscaffolds allowed better control over the bioassembly potential, independent of the maturation period. Our approach enables to utilize building blocks of high degree of maturity (e.g. differentiated cartilage units), which can still assemble into a cohesive tissue-construct. Further investigations are still needed to decipher which biological stimulus is triggered by the presence of the microscaffold, enabling S-SPHs to preserve such robust fusiogenicity otherwise lost when only SPHs are used.

4.2. S-SPHs bioassemble into a tissue construct, while avoiding excessive compaction

Spheroids put in close contact to each other naturally and spontaneously fuse like “liquid droplets”, forming a spherical tissue, trying to minimize their interfacial area [32]. This compaction makes the fabrication of reproducible and standardize SPHs on a large scale, as well as complex 3D tissues built from such SPHs extremely difficult. Many examples facing this issue are available in the literature, with for instance Napolitano et al. who created a toroid-like structure based on multiple self-assembled spheroids. Within 5 days, only 33 % of those structures retained their toroid-like shape, whereas the majority retracted and aggregated to become spherical [33]. Similarly, Olsen et al. reported on similar ring-like structure resulting from the self-assembly of multiple spheroids. Within less than one week the ring-like structure compacted into a spheroid tissue, due to the forces generated through cell-cell and cell-ECM interaction [34]. They also observed that the lower the initial number of cells used to create each SPH, the faster the compaction was. Self-assembled tissues from spheroids based on 5000 cells compacted more than 30 % within 48 h of culture. Similarly, Parfenov et al. fabricated spheroids of 1.6×10^4 cells, and measured a size reduction of doublets of more than 70 % with 24 h [35]. We used the exact same seeding density per SPH as in Olsenś study (i.e. 5000 hASC) and our results from the doublet experiments, correlated with this previous observation. However, this can be significantly countered when using S-SPH instead of SPH.

Due to the intense compaction happening upon maturation of SPHs, the size of both, the single SPHs and the resulting merged tissue undergo drastic reduction. This compaction further leads to

the reduction in size of the bioassembled tissue over time of cultivation. Based on our experiment, if we consider that a freshly prepared SPH (week 0) has a diameter of 350 µm (corresponding to a volume of 0,045 mm^3 for a doublet), and that after a maturation of 2 weeks, a SPH doublet cultured for 7 days has a total length of 250 µm (corresponding to a volume of 0,008 mm^3), the volume reduces by a factor greater than 5. Similar calculation made from S-SPH doublet would correspond to a decrease of 1.8 times and of only 1.2 times if we exclude the mass of cells surrounding the microscaffold. From our set of experiment, it is clear that S-SPHs offer a better control over the size of the bioassembled tissue-constructs. This can be further highlighted by the conducted "TU-shaped" defect experiments, where a defined volume could be precisely filled with a calculated number of S-SPHs, while at least 11 % of volume remained empty after 6 h of culturing when SPHs were used. This furthermore shows the advantage of lower degree of shrinkage of S-SPHs compared to SPHs while preserving the possibility of filling up complex shaped defects.

The quality of the formed tissue is not only dependent on the size evolution of each building block, but more importantly, on it's degree of maturation. For instance, Rago et al. produced rods based on multiple spheroids and observed an intensity of the tissue compaction inversely proportional to the degree of maturation of the cells [20]. He showed that the fusiogenicity of doublets was also decreasing by prolonging the maturation of the SPHs. Preculturing spheroids for 1 day resulted in a sphere-like structure upon self-assembly. Repeating this experiment with 7-day old doublets formed tissues where both SPHs were still discernible. In opposition to many authors [20,33,34], we did not observe that the degree of maturation exerted any effects neither on the fusiogenicity of the S-SPH, and more importantly, nor on the final size of the merged structures.

4.3. S-SPHs alleviate present limitations of SPH-based approaches

The opportunity offered by this third strategy in tissue engineering with the possibility to mix cellularized and empty microscaffolds, which composition still possesses bioassembly behaviour, permits to control the final cell density of the tissue construct. This property comes most probably due to the design of the microscaffold, with it's thin strut sizes and high degree of porosity, enabling cells from S-SPHs to easily migrate and colonize the surrounding empty microscaffolds within a few days. This underlines that the third tissue engineering strategy has a great versatility to be used in the future as minimally invasive approach, in order to fill up defects of defined volume with a desired cellular density. The ratio of S-SPHs / empty microscaffolds to be delivered can be adapted to the physiological activity of the required tissues, as some are known to contain naturally high number of cells (like bone), while other tissues are poorly cellularized and consequently cannot sustain an exogenous addition of too many cells (like cartilage or intervertebral disks (IVDs)). This opportunity might extend the field of spheroid-based therapy to tissues so far excluded due to their inadequate natural cell density, too low to sustain the viability and the functionality of transplanted SPHs.

Tissue engineering constructs resulting from the assembly of multiple SPHs are also limited in size due to the difficulty for the cells present in the core to have access to nutrient and oxygen. Vascularization is often proposed as generic answer to such issues, even though i- pre-vascularizing an engineered tissue *in vitro* remains highly challenging [36–38], and that ii- some tissues are naturally avascular (e.g. articular cartilage, IVDs, skin epithelium, cornea, or even meniscus and tendon to a lower degree to cite just a few). By using combination of S-SPHs and empty microscaffolds, we could obtain tissue-constructs of similar or even larger size compared to the use of S-SPHs only, but with a significantly reduced density of cells. This new opportunity, unique to this third tissue engineering strategy, could potentially alleviate the urgent need of tissue vascularization and enhance the survival of cells post-implantation.

A last aspect that would deserve further investigation is the self-compartmentalization of cells occurring upon spheroid fusion (also called self-sorting) [20]. Indeed, upon self-assembly of spheroids composed of heterogeneous cell types, cells will self-organize into the newly created tissue, where one type usually forms the inner core and the other the outer layer, in a phenomenon called the differential adhesion hypothesis (DAH) [39,40]. This compartmentalization has been observed by many reports [20,41], and is a fundamental principle of developmental biology [40]. We might nevertheless hypothesise that for specific applications focusing on heterogeneous tissues, being able to control and even limit this compartmentalization would be favourable. This would for example be beneficial when heterotypic SPHs are to be used to regenerate an osteo-chondral tissue with zonal repartition of bone cells and cartilage cells. Similar segregation might be required to recreate *in vitro* tissues like the ovarian follicle characterized by oocyte surrounded by layers of granulose and theca cells [42], or the epidermal/dermal layers of the skin. Even though we have not elucidated this aspect, it is probable that the presence of microscaffolds, which inhibits the compaction, also limits the phenomenon of self-compartmentalization to a certain degree. If this aspect is validated, we could envision to regenerate for instance an osteo-chondral defect, by injecting consecutively matured osteogenic S-SPHs followed by chondrogenic S-SPHs, that will subsequently bioassemble *in situ* into a cohesive and already differentiated tissue.

4.4. Perspectives of S-SPH for cartilage tissue engineering

In situ repair of cartilage lesions using bottom-up approaches in TERM, via micro-size building blocks are currently under vivid research. Literature analysis conducted by Grottkau et al. emphazised that "micro-cartilage bioassembly" is a young and also a robust growing thematic in scientific publication [43]. Nonetheless, recurrent drawbacks still limit the size of the cartilage tissue one can fabricate via bioassembly of micro-cartilage units. Indeed, spheroids can fuse only into a small and thin tissue (< 0.75 mm in height) [44], and attempts to up-scale this dimension are generally troublesome due to the limited fusiogenic properties of the building blocks, the resulting poor mechanical properties and the formation of a necrotic core. Having shown in this publication that the fusiogenicity of S-SPH is not dependent on their degree of maturation and that chondrogenic S-SPH can form a cohesive tissue, not achievable using SPH, the proposed third tissue engineering strategy offers great perspective for bioassembly of cartilage tissue repair.

The usage of MPL processes for TERM application is often criticized due to the long printing time requires to fabricate macro-size constructs. Our group is actively tackling this bottleneck, and we have shown for instance in 2020 the capability of our MPL system to print large-size scaffolds with volumes one order of magnitude bigger than any other previous report [45]. This was made possible thanks to the selection of highly photo-reactive resins together with a fast printing speed (1000 $m.s^{-1}$). In our more recent publication, we have discussed that the printing time required to produce enough microscaffolds to fill up a $1cm^3$ cartilage defect would require 6 days [18]. Furthermore, continuous research in the field of two-photon-polymerization could result in improved 2PP systems capable of reducing the printing time further and allow upscaling of the microscaffold fabrication in the near future.

Taking into consideration the possibility to automatize the entire work-flow consisting on 1- printing, 2-post-printing development (i.e. washing steps required to remove the non-polymerized resin), 3- individualization of each microscaffold into single well (doable using a Biosorter (e.g. commercialized by Unionbio, Aalst Belgium), 4- sterilization (i.e. 30 min UV-sterilization cycle) and finally the deposition of patient cells and their agglomeration with each microscaffold (requiring generally 48 h), the time required for the fabrication of S-SPH does not seem anymore being such a strong constrain.

4.5. New technology calls for new definition

Athanasiou et al. defined "self-assembly" as "a process in tissue engineering using scaffoldless technology which produces tissues that demonstrate spontaneous organization without external forces" [46]. Later on, Groll et al. and Moroni et al., included the possibility of "pre-formed cell-containing fabrication units, i.e. hybrid cell-material building blocks" to an adapted "bioassembly" terminology [47,48]. This new publication is a great example on how bioassembly of such hybrid cell-material building blocks can be used in bottom-up tissue engineering strategies, revealing clear advantages over conventional self-assembled spheroids. According to the definition of "spheroid" proposed by Fennema et al., as a "small aggregate of cells growing free from foreign materials" [30], we propose a new concept of "scaffolded spheroid" intrinsic to this third tissue engineering strategy, being "a small aggregate of cells growing within a micro-size scaffold, maintaining bioassembly behaviour", as utilized in this manuscript.

5. Conclusion

The third tissue engineering strategy offers unprecedented opportunities by unifying scaffold-free and scaffold-based strategies. We have recently shown the possibility to create multiple building blocks by integrating single spheroids within microscaffolds. For this new strategy to become a breakthrough in tissue engineering, it is not only important to demonstrate that high number of S-SPHs can be rapidly produced, but that they possess unaltered stemness potential and robust fusiogenic properties. This is a strong prerequisite, since building blocks with poor, unreproducible or uncontrollable self-assembly properties cannot be used further as building blocks to engineer large tissue structures.

Collectively, we have shown that the fusiogenic potentials of S-SPHs is not only unaltered by the presence of microscaffolds compared to SPH, but that some aspects are even favoured. Indeed, the size of tissues formed by S-SPHs fusing together is more stable over time compared to normal spheroids, and independent of their degree of maturation. Both freshly formed or matured S-SPHs exhibit almost the same fusiogenicity, which was so far the most important limiting factor intrinsic to normal SPHs. Finally, our last experiments seem to indicate that this advantage is conferred due to the higher migration potential of the cells present at the surface of S-SPHs. Being able to engineer building blocks with reproducible fusiogenicity, uncoupled from their degree of maturation, and from the initial cellular loading density, offer a significant simplicity and advantages over spheroid-based therapies for tissue regeneration. Tissues with high degree of maturity like cartilage can now be produced by the bioassembly of chondrogenically differentiated S-SPHs, not achievable using scaffold-free SPHs.

Finally, as new technologies need new definitions, we propose to adapt the existing terminology in the field and to introduce the term of "scaffolded spheroid", being "a small aggregate of cells growing within a micro-size scaffold, maintaining bioassembly behaviour".

Declaration of Competing Interest

The authors declare that they have no known competing financial interests or personal relationships that could have appeared to influence the work reported in this paper.

Acknowledgment

This project has received funding from the European Research Council (ERC) under the European Union's Horizon 2020 research and innovation programme (Grant agreement No. 772464).

Supplementary materials

Supplementary material associated with this article can be found, in the online version, at doi:10.1016/j.actbio.2023.12.001.

References

[1] E.A. Bulanova, E.V. Koudan, J. Degosserie, C. Heymans, F.D. Pereira, V.A. Parfenov, Y. Sun, Q. Wang, S.A. Akhmedova, I.K. Sviridova, N.S. Sergeeva, G.A. Frank, Y.D. Khesuani, C.E. Pierreux, V.A. Mironov, Bioprinting of a functional vascularized mouse thyroid gland construct, Biofabrication 9 (2017) 034105, doi:10.1088/1758-5090/aa7fdd.
[2] V. Mironov, R.P. Visconti, V. Kasyanov, G. Forgacs, C.J. Drake, R.R. Markwald, Organ printing: tissue spheroids as building blocks, Biomaterials 30 (2009) 2164–2174, doi:10.1016/j.biomaterials.2008.12.084.
[3] B.S. Schon, G.J. Hooper, T.B.F. Woodfield, Modular tissue assembly strategies for biofabrication of engineered cartilage, Ann. Biomed. Eng. 45 (2017) 100–114, doi:10.1007/s10439-016-1609-3.
[4] J.H. Jeon, B.G. Yun, M.J. Lim, S.J. Kim, M.H. Lim, J.Y. Lim, S.H. Park, S.W. Kim, Rapid cartilage regeneration of spheroids composed of human nasal septum-derived chondrocyte in rat osteochondral defect model, Tissue Eng Regen Med 17 (2020) 81–90, doi:10.1007/s13770-019-00231-w.
[5] M. Zhang, J. Shi, M. Xie, J. Wen, K. Niibe, X. Zhang, J. Luo, R. Yan, Z. Zhang, H. Egusa, X. Jiang, Recapitulation of cartilage/bone formation using iPSCs via biomimetic 3D rotary culture approach for developmental engineering, Biomaterials 260 (2020) 120334, doi:10.1016/j.biomaterials.2020.120334.
[6] V. Mironov, J. Zhang, C. Gentile, K. Brakke, T. Trusk, K. Jakab, G. Forgacs, V. Kasyanov, R.P. Visconti, R.R. Markwald, Designer 'blueprint' for vascular trees: morphology evolution of vascular tissue constructs, Virtual Phys. Prototyp. 4 (2009) 63–74, doi:10.1080/17452750802657202.
[7] M. Stadler, M. Scherzer, S. Walter, S. Holzner, K. Pudelko, A. Riedl, C. Unger, N. Kramer, B. Weil, J. Neesen, M. Hengstschläger, H. Dolznig, Exclusion from spheroid formation identifies loss of essential cell-cell adhesion molecules in colon cancer cells, Sci. Rep. 8 (2018) 1151, doi:10.1038/s41598-018-19384-0.
[8] S.J. Han, S. Kwon, K.S. Kim, Challenges of applying multicellular tumor spheroids in preclinical phase, Cancer Cell Int. 21 (2021) 152, doi:10.1186/s12935-021-01853-8.
[9] N.P. Omelyanenko, P.A. Karalkin, E.A. Bulanova, E.V. Koudan, V.A. Parfenov, S.A. Rodionov, A.D. Knyazeva, V.A. Kasyanov, I. Babichenko, T.Z. Chkadua, Y.D. Khesuani, A.A. Gryadunova, V.A. Mironov, Extracellular matrix determines biomechanical properties of chondrospheres during their maturation in vitro, Cartilage 11 (2020) 521–531, doi:10.1177/1947603518798890.
[10] P.D. Dalton, T.B.F. Woodfield, V. Mironov, J. Groll, Advances in hybrid fabrication toward hierarchical tissue constructs, Adv. Sci. 7 (2020) 1902953, doi:10.1002/advs.201902953.
[11] T. Ahmad, J. Lee, Y.M. Shin, H.J. Shin, S.K. Madhurakat Perikamana, S.H. Park, S.W. Kim, H. Shin, Hybrid-spheroids incorporating ECM like engineered fragmented fibers potentiate stem cell function by improved cell/cell and cell/ECM interactions, Acta Biomater. 64 (2017) 161–175, doi:10.1016/j.actbio.2017.10.022.
[12] T. Ahmad, H.J. Shin, J. Lee, Y.M. Shin, S.K.M. Perikamana, S.Y. Park, H.S. Jung, H. Shin, Fabrication of in vitro 3D mineralized tissue by fusion of composite spheroids incorporating biomineral-coated nanofibers and human adipose-derived stem cells, Acta Biomater. 74 (2018) 464–477, doi:10.1016/j.actbio.2018.05.035.
[13] G. Hong, J. Kim, H. Oh, S. Yun, C.M. Kim, Y.-M. Jeong, W.-S. Yun, J.-H. Shim, I. Jang, C.-Y. Kim, S. Jin, Production of multiple cell-laden microtissue spheroids with a biomimetic hepatic-lobule-like structure, Adv. Mater. 33 (2021) 2102624, doi:10.1002/adma.202102624.
[14] M.C. Decarli, A. Seijas-Gamardo, F.L.C. Morgan, P. Wieringa, M.B. Baker, J.V.L. Silva, Â.M. Moraes, L. Moroni, C. Mota, Bioprinting of stem cell spheroids followed by post-printing chondrogenic differentiation for cartilage tissue engineering, Adv. Healthc. Mater. (2023) 2203021, doi:10.1002/adhm.202203021.
[15] N.I. Moldovan, N. Hibino, K. Nakayama, Principles of the *Kenzan* method for robotic cell spheroid-based three-dimensional bioprinting <sup/>, Tissue Eng. Part B 23 (2017) 237–244, doi:10.1089/ten.teb.2016.0322.
[16] N.V. Mekhileri, K.S. Lim, G.C.J. Brown, I. Mutreja, B.S. Schon, G.J. Hooper, T.B.F. Woodfield, Automated 3D bioassembly of micro-tissues for biofabrication of hybrid tissue engineered constructs, Biofabrication 10 (2018) 024103, doi:10.1088/1758-5090/aa9ef1.

[17] A. Ovsianikov, A. Khademhosseini, V. Mironov, The synergy of scaffold-based and scaffold-free tissue engineering strategies, Trends Biotechnol. 36 (2018) 348–357, doi:10.1016/j.tibtech.2018.01.005.
[18] O. Guillaume, O. Kopinski-Grünwald, G. Weisgrab, T. Baumgartner, A. Arslan, K. Whitmore, S. Van Vlierberghe, A. Ovsianikov, Hybrid spheroid microscaffolds as modular tissue units to build macro-tissue assemblies for tissue engineering, Acta Biomater. (2022) S1742706122001416, doi:10.1016/j.actbio.2022.03.010.
[19] K.R. Silva, R.A. Rezende, F.D.A.S. Pereira, P. Gruber, M.P. Stuart, A. Ovsianikov, K. Brakke, V. Kasyanov, J.V.L. da Silva, J.M. Granjeiro, L.S. Baptista, V. Mironov, Delivery of human adipose stem cells spheroids into lockyballs, PLoS One 11 (2016) e0166073, doi:10.1371/journal.pone.0166073.
[20] A.P. Rago, D.M. Dean, J.R. Morgan, Controlling cell position in complex heterotypic 3D microtissues by tissue fusion, Biotechnol. Bioeng. 102 (2009) 1231–1241, doi:10.1002/bit.22162.
[21] G.S. Kronemberger, A. Beatrici, G.M.L. Dalmônico, A.L. Rossi, G.A.S.C. Miranda, L.C. Boldrini, J.M. Granjeiro, L.S. Baptista, The hypertrophic cartilage induction influences the building-block capacity of human adipose stem/stromal cell spheroids for biofabrication, Artif. Organs 45 (2021) 1208–1218, doi:10.1111/aor.14000.
[22] N.V. Kosheleva, Y.M. Efremov, B.S. Shavkuta, I.M. Zurina, D. Zhang, Y. Zhang, N.V. Minaev, A.A. Gorkun, S. Wei, A.I. Shpichka, I.N. Saburina, P.S. Timashev, Cell spheroid fusion: beyond liquid drops model, Sci. Rep. 10 (2020) 12614, doi:10.1038/s41598-020-69540-8.
[23] A. Ajami, W. Husinsky, M. Tromayer, P. Gruber, R. Liska, A. Ovsianikov, Measurement of degenerate two-photon absorption spectra of a series of developed two-photon initiators using a dispersive white light continuum Z-scan, Appl. Phys. Lett. 111 (2017) 071901, doi:10.1063/1.4989917.
[24] L. Knezevic, M. Schaupper, S. Mühleder, K. Schimek, T. Hasenberg, U. Marx, E. Priglinger, H. Redl, W. Holnthoner, Engineering blood and lymphatic microvascular networks in fibrin matrices, Front. Bioeng. Biotechnol. 5 (2017), doi:10.3389/fbioe.2017.00025.
[25] S. Žigon-Branc, M. Markovic, J. Van Hoorick, S. Van Vlierberghe, P. Dubruel, E. Zerobin, S. Baudis, A. Ovsianikov, Impact of hydrogel stiffness on differentiation of human adipose-derived stem cell microspheroids, Tissue Eng. Part A 25 (2019) 1369–1380, doi:10.1089/ten.tea.2018.0237.
[26] J. Schindelin, I. Arganda-Carreras, E. Frise, V. Kaynig, M. Longair, T. Pietzsch, S. Preibisch, C. Rueden, S. Saalfeld, B. Schmid, J.-Y. Tinevez, D.J. White, V. Hartenstein, K. Eliceiri, P. Tomancak, A. Cardona, Fiji: an open-source platform for biological-image analysis, Nat. Methods 9 (2012) 676–682, doi:10.1038/nmeth.2019.
[27] O. Kopinski-Grünwald, Automated Region of interest (ROI) finder based on the fluorescent signal of cellular spheroids for image analysis to study cell migration, (2023). 10.48436/dkvqb-1qz17.
[28] R.C. Hibbeler, Mechanics of Materials, 8th ed., Prentice Hall, Boston, 2011.
[29] G.C.J. Lindberg, X. Cui, M. Durham, L. Veenendaal, B.S. Schon, G.J. Hooper, K.S. Lim, T.B.F. Woodfield, Probing multicellular tissue fusion of cocultured spheroids—a 3D-bioassembly model, Adv. Sci. 8 (2021) 2103320, doi:10.1002/advs.202103320.
[30] E. Fennema, N. Rivron, J. Rouwkema, C. van Blitterswijk, J. de Boer, Spheroid culture as a tool for creating 3D complex tissues, Trends Biotechnol. 31 (2013) 108–115, doi:10.1016/j.tibtech.2012.12.003.
[31] G.N. Hall, I. Rutten, J. Lammertyn, J. Eberhardt, L. Geris, F.P. Luyten, I. Papantoniou, Cartilaginous spheroid-assembly design considerations for endochondral ossification: towards robotic-driven biomanufacturing, Biofabrication 13 (2021) 045025, doi:10.1088/1758-5090/ac2208.
[32] K. Jakab, C. Norotte, B. Damon, F. Marga, A. Neagu, C.L. Besch-Williford, A. Kachurin, K.H. Church, H. Park, V. Mironov, R. Markwald, G. Vunjak-Novakovic, G. Forgacs, Tissue engineering by self-assembly of cells printed into topologically defined structures, Tissue Eng. Part A 14 (2008) 413–421, doi:10.1089/tea.2007.0173.
[33] A.P. Napolitano, P. Chai, D.M. Dean, J.R. Morgan, Dynamics of the self-assembly of complex cellular aggregates on micromolded nonadhesive hydrogels, Tissue Eng. 13 (2007) 2087–2094, doi:10.1089/ten.2006.0190.
[34] T.R. Olsen, B. Mattix, M. Casco, A. Herbst, C. Williams, A. Tarasidis, D. Simionescu, R.P. Visconti, F. Alexis, Manipulation of cellular spheroid composition and the effects on vascular tissue fusion, Acta Biomater. 13 (2015) 188–198, doi:10.1016/j.actbio.2014.11.024.
[35] V.A. Parfenov, E.V. Koudan, A.A. Krokhmal, E.A. Annenkova, S.V. Petrov, F. Pereira, P.A. Karalkin, E.K. Nezhurina, A.A. Gryadunova, E.A. Bulanova, O.A. Sapozhnikov, S.A. Tsysar, K. Liu, E. Oosterwijk, H. van Beuningen, P. van der Kraan, S. Granneman, H. Engelkamp, P. Christianen, V. Kasyanov, Y.D. Khesuani, V.A. Mironov, Biofabrication of a functional tubular construct from tissue spheroids using magnetoacoustic levitational directed assembly, Adv. Healthc. Mater. 9 (2020) e2000721, doi:10.1002/adhm.202000721.
[36] A.W.L. Liew, Yilei Zhang, In vitro pre-vascularization strategies for tissue engineered constructs-bioprinting and others, Int. J. Bioprint. 3 (2017) 008–008, doi:10.18063/IIB.2017.01.008.
[37] L. De Moor, J. Smet, M. Plovyt, B. Bekaert, C. Vercruysse, M. Asadian, N. De Geyter, S. Van Vlierberghe, P. Dubruel, H. Declercq, Engineering microvasculature by 3D bioprinting of prevascularized spheroids in photo-crosslinkable gelatin, Biofabrication 13 (2021) 045021, doi:10.1088/1758-5090/ac24de.
[38] M. Rahimnejad, N. Nasrollahi Boroujeni, S. Jahangiri, N. Rabiee, M. Rabiee, P. Makvandi, O. Akhavan, R.S. Varma, Prevascularized micro-/nano-sized spheroid/bead aggregates for vascular tissue engineering, Nano-Micro Lett. 13 (2021) 182, doi:10.1007/s40820-021-00697-1.
[39] R.A. Foty, C.M. Pfleger, G. Forgacs, M.S. Steinberg, Surface tensions of embryonic tissues predict their mutual envelopment behavior, Development 122 (1996) 1611–1620, doi:10.1242/dev.122.5.1611.
[40] R.A. Foty, M.S. Steinberg, The differential adhesion hypothesis: a direct evaluation, Dev. Biol. 278 (2005) 255–263, doi:10.1016/j.ydbio.2004.11.012.
[41] R.F.X. Tomasi, S. Sart, T. Champetier, C.N. Baroud, Individual control and quantification of 3d spheroids in a high-density microfluidic droplet array, Cell Rep. 31 (2020) 107670, doi:10.1016/j.celrep.2020.107670.
[42] P.K. Kreeger, J.W. Deck, T.K. Woodruff, L.D. Shea, The in vitro regulation of ovarian follicle development using alginate-extracellular matrix gels, Biomaterials 27 (2006) 714–723, doi:10.1016/j.biomaterials.2005.06.016.
[43] B.E. Grottkau, Z. Hui, Y. Pang, Articular cartilage regeneration through bioassembling spherical micro-cartilage building blocks, Cells 11 (2022) 3244, doi:10.3390/cells11203244.
[44] A.D. Dikina, D.S. Alt, S. Herberg, A. McMillan, H.A. Strobel, Z. Zheng, M. Cao, B.P. Lai, O. Jeon, V.I. Petsinger, C.U. Cotton, M.W. Rolle, E. Alsberg, A modular strategy to engineer complex tissues and organs, Adv. Sci. 5 (2018) 1700402, doi:10.1002/advs.201700402.
[45] G. Weisgrab, O. Guillaume, Z. Guo, P. Heimel, P. Slezak, A. Poot, D. Grijpma, A. Ovsianikov, 3D Printing of large-scale and highly porous biodegradable tissue engineering scaffolds from poly(trimethylene-carbonate) using two-photon-polymerization, Biofabrication 12 (2020) 045036, doi:10.1088/1758-5090/abb539.
[46] K.A. Athanasiou, R. Eswaramoorthy, P. Hadidi, J.C. Hu, Self-organization and the self-assembling process in tissue engineering, Annu. Rev. Biomed. Eng. 15 (2013) 115–136, doi:10.1146/annurev-bioeng-071812-152423.
[47] J. Groll, T. Boland, T. Blunk, J.A. Burdick, D.-W. Cho, P.D. Dalton, B. Derby, G. Forgacs, Q. Li, V.A. Mironov, L. Moroni, M. Nakamura, W. Shu, S. Takeuchi, G. Vozzi, T.B.F. Woodfield, T. Xu, J.J. Yoo, J. Malda, Biofabrication: reappraising the definition of an evolving field, Biofabrication 8 (2016) 013001, doi:10.1088/1758-5090/8/1/013001.
[48] L. Moroni, T. Boland, J.A. Burdick, C. De Maria, B. Derby, G. Forgacs, J. Groll, Q. Li, J. Malda, V.A. Mironov, C. Mota, M. Nakamura, W. Shu, S. Takeuchi, T.B.F. Woodfield, T. Xu, J.J. Yoo, G. Vozzi, Biofabrication: a guide to technology and terminology, Trends Biotechnol. 36 (2018) 384–402, doi:10.1016/j.tibtech.2017.10.015.